A Journal of the Gesellschaft Deutscher Chemiker

Angewandte International Edition

GDCh

Chemie

www.angewandte.org

Accepted Article

Title: Electro-active pure organic room-temperature phosphorescence polymer based on a donor-oxygen-acceptor geometry

Authors: Junqiao Ding

To be cited as: *Angew. Chem. Int. Ed.* 10.1002/anie.202011957

Link to VoR: https://doi.org/10.1002/anie.202011957

WILEY-VCH

10.1002/anie.202011957

WILEY-VCH

Electro-active pure organic room-temperature phosphorescence polymer based on a donor-oxygen-acceptor geometry

Xinrui Liu, Liuqing Yang, Xuefei Li, Lei Zhao, Shumeng Wang, Zheng-Hong Lu,* Junqiao Ding,* Lixiang Wang*

Abstract: Amorphous polymers showing pure organic room-temperature phosphorescence (RTP) have emerged as an attractive alternative to crystalline small molecular phosphors due to their ease of film preparation and compatibility with flexible electronics. However, the current reported RTP polymers are electrically insulating, and unable to be used to fabricate practical optoelectronic devices that require charge transporting capability to some degree. Here we demonstrate an electro-active RTP polymer based on a characteristic donor-oxygen-acceptor geometry. Compared with the donor-acceptor reference, the inserted oxygen atom between donor and acceptor can not only decrease hole-electron orbital overlap to suppress the charge transfer fluorescence, but also strengthen spin-orbital coupling effect to facilitate the intersystem crossing and subsequent phosphorescence channels. As a result, a significant RTP is observed in solid states under photo excitation. Most noticeably, the corresponding polymer light-emitting diodes (PLEDs) reveal a dominant electrophosphorescence with a record-high external quantum efficiency of 9.7%. The performance goes well beyond the 5% theoretical limit for typical fluors, opening a new door to the development of pure organic RTP polymers towards efficient PLEDs.

1. Introduction

Recently pure organic room-temperature phosphorescence (RTP) luminophores have drawn extensive attention because of the intrinsic low cost, wide tunable functionality, negligible cytotoxicity and good processibility[1-4]. Compared with metal-containing inorganic and organometallic complexes, obtaining a strong RTP in pure organic materials is much more challenging due to inefficient intersystem crossing (ISC) caused by the weak spin-orbital coupling (SOC) and ultrafast nonradiative decay of triplet excitons[5]. Therefore, a variety of methodologies are proposed to develop RTP small molecules, such as non-covalent interactions (hydrogen and halogen bonding)[6-9], heavy atom effect[10,11], H-aggregation[12-14] and n-π transition[15,16]. However, they often rely on crystal engineering to prevent molecular vibrations and nonradiative deactivation[17]. The required critical growth condition inevitably leads to difficulty in preparing high-quality and reliable films for practical applications, such as organic optoelectronic devices[18], encryption and anti-counterfeit data security[19].

To address this problem, amorphous RTP polymers[20,21], which are believed to be more applicable and compatible with the flexible electronics (flexible and stretchable, lightweight, solution processing etc.)[22], have been designed by incorporating phosphors into polymer matrixes via physical encapsulation, covalent attachment and crosslinking[23-29]. In this case, the intertwined structure of polymers can not only provide a rigid environment to immobilize the phosphors for a suppressed nonradiative transition[24], but also isolate oxygen and humidity to avoid triplet exciton quenching[20]. Consequently, RTP polymers are able to emit bright phosphorescence under photo excitation. Nevertheless, their electrophosphorescence device applications under electric excitation have been seldomly reported so far[30]. The main reason is that these RTP polymers are not suitable for polymer light-emitting diodes (PLEDs)[31-33], because most of used polymer matrixes including poly(methyl methacrylate) (PMMA)[23,24], poly(vinyl alcohol) (PVA)[19,25], poly(lactic acid) (PLA)[26,27] and poly(acrylamide) (PAM)[28,29] are electrically insulating.

Here, we demonstrate an electro-active RTP polymer named P(DMPAc-O-TPTrz) for efficient PLEDs (Figure 1), where an oxygen atom (O) is inserted as the spacer between the acridine donor (D) and triazine acceptor (A). Benefitting from the characteristic D-O-A geometry, the hole-electron orbital overlap is found to be decreased to suppress the charge transfer (CT) fluorescence. Meanwhile, the introduced O can strengthen the SOC effect, and facilitate the spin flipping from the lowest singlet state (S_1) to triplet states (T_n) and then to the ground state (S_0). As a result, a considerable RTP component is observed under photo excitation for the neat and doped films of P(DMPAc-O-TPTrz). This is quite different from the D-A based counterpart P(DMPAc-TPTrz), which shows only fluorescence. Most noticeably, P(DMPAc-O-TPTrz) achieves a dominant electrophosphorescence with a record-high external quantum efficiency (EQE) of 9.7% (24.0 cd/A, 18.9 lm/W) and Commission Internationale de L'Eclairage (CIE) coordinates of (0.27, 0.41). The value surpasses the 5% theoretical limit for typical fluors, clearly demonstrating the great potential of pure organic RTP polymers in efficient PLEDs.

[*] X. Liu, L. Yang, X. Li, Dr. L. Zhao, Dr. S. Wang, Prof. J. Ding, Prof. L. Wang
State Key Laboratory of Polymer Physics and Chemistry
Changchun Institute of Applied Chemistry
Chinese Academy of Sciences, Changchun 130022, P. R. China
E-mail: wangshumeng@ciac.ac.cn
X. Liu, L. Yang, X. Li, Prof. J. Ding, Prof. L. Wang
University of Science and Technology of China
Hefei 230026, P. R. China
X. Liu, L. Yang, X. Li, Prof. J. Ding
School of Chemical Science and Technology, Yunnan University
Kunming 650091, P. R. China
E-mail: dingjunqiao@ynu.edu.cn
Prof. Z.-H. Lu
Department of Materials Science and Engineering
University of Toronto, Toronto, Ontario, Canada
E-mail: zhenghong.lu@utoronto.ca

Supporting information for this article is given via a link at the end of the document.

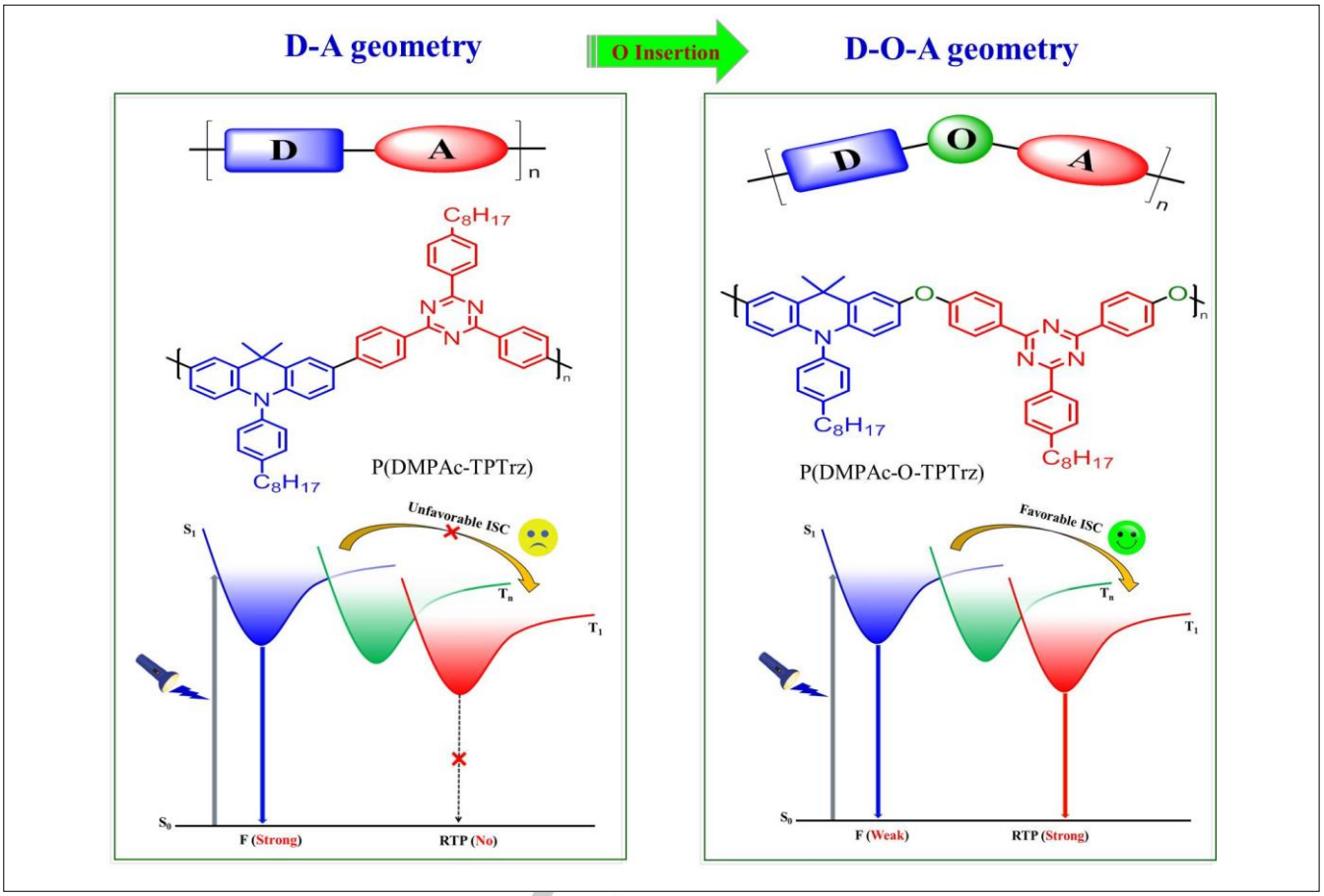

Figure 1. Molecular design from fluorescence polymers with a D-A geometry to pure organic RTP polymers with a D-O-A geometry. F: fluorescence; RTP: room-temperature phosphorescence; ISC: intersystem crossing.

Table 1. Photophysical, electrochemical and thermal properties of P(DMPAc-TPTrz) and P(DMPAc-O-TPTrz).

	λ_{abs} [a] [nm]	λ_{PL} [b] [nm]	FWHM [b] [nm]	λ_P at 77 K/RT [c] [nm]	Φ_{PL} [d] [%]	τ_F [e] [ns]	τ_P [e] [ns]	HOMO/LUMO [f] [eV]	E_g [g] [eV]	T_g [h] [°C]	T_d [h] [°C]
P(DMPAc-TPTrz)	292, 408	491 (488)	61 (55)	573/n.d. (569/n.d.)	9.0 (29.7)	3.9 (4.1)	n.d. (n.d.)	-5.38/-2.65	2.74/2.73	n.d.	390
P(DMPAc-O-TPTrz)	298	486 (479)	99 (91)	490/505 (484/487)	21.4 (49.5)	17.8 (15.1)	825.4 (1642.6)	-5.47/-2.52	3.01/2.95	129	428

[a]Absorption measured in 10^{-5} mol L^{-1} toluene solution. [b]Steady-state PL at room temperature measured in neat films. [c]Phosphorescence measured in neat films with a 2 ms (77 K) or 0.05 ms (room temperature) delay time between the pulsed excitation and the emission collection. [d]PLQY measure in neat films under N_2 using an integral sphere. [e]Fluorescence and phosphorescence lifetimes estimated from the transient PL spectra. [f]HOMO = -e[$E_{onset,\ ox}$ + 4.8 V], LUMO = -e[$E_{onset,\ red}$ + 4.8 V], where $E_{onset,\ ox}$ and $E_{onset,\ red}$ are the onset values of the first oxidation and reduction waves, respectively. [g]Optical and electrochemical band gap. [h]Glass transition temperature and decomposition temperature determined from DSC and TGA. All data listed in the parentheses are for the 15 wt.% doped films in mCP.

2. Results and Discussion

2.1 Synthesis and characterization

The synthesis of the target RTP polymer P(DMPAc-O-TPTrz) is shown in Scheme S1. Starting from 9,9-dimethyl-9,10-dihydroacridine, bromination, methoxyl exchange, C-N coupling and demethylation were carried out in sequence to produce the dihydroxy monomer **M1**. On the other hand, the difluoro monomer **M2** was prepared from 2,4,6-trichloro-1,3,5-triazine by a two-step C-C coupling process. Finally, a nucleophilic aromatic substitution polymerization[32] between **M1** and **M2** was performed to afford P(DMPAc-O-TPTrz) with a D-O-A geometry. For comparison, the reference polymer P(DMPAc-TPTrz) with a D-A geometry was simultaneously synthesized via a Suzuki polymerization[33]. Their molecular structures were thoroughly characterized by ^{1}H and ^{13}C NMR, elementary analysis and gel permeation chromatography (GPC). The number-average molecular weight (Mn) and polydispersity index (PDI) are determined to be 10.6 kDa and 3.6 for P(DMPAc-O-TPTrz) and 7.3 kDa and 1.8 for P(DMPAc-TPTrz). Compared to P(DMPAc-TPTrz), the O-induced backbone torsion (Figure S1) endows P(DMPAc-O-TPTrz) with a larger Mn and better solubility in common organic solvents, such as toluene, chloroform, chlorobenzene and tetrahydrofuran. Also, P(DMPAc-O-TPTrz) is thermally stable (Figure S2), displaying a distinct glass transition temperature (T_g = 129 °C) and a higher decomposition temperature (T_d = 428 °C) than that of P(DMPAc-TPTrz) (T_d = 390 °C).

2.2 Electrochemical properties

Cyclic voltammetry (CV) was used to study their electrochemical properties. Similar to P(DMPAc-TPTrz) (Figure S3), a quasi-reversible oxidation and reduction waves occur for P(DMPAc-O-TPTrz) during the anodic and cathodic sweeping. This is an indicator of the electro-active feature for P(DMPAc-O-TPTrz), which is beneficial for charge transporting in PLEDs[34]. With ferrocene/ferrocenium (Fc/Fc^{+}) as the reference (4.8 eV under vacuum), moreover, the highest occupied and lowest unoccupied molecular orbital (HOMO/LUMO) energy levels of P(DMPAc-O-TPTrz) are taken to be -5.47 and -2.52 eV, respectively. Owing to the oxygen insertion between D and A, the backbone conjugation is anticipated to be disrupted to some degree, resulting in a decreased HOMO and an increased LUMO relative to P(DMPAc-TPTrz) (HOMO = -5.38 eV, LUMO = -2.65 eV).

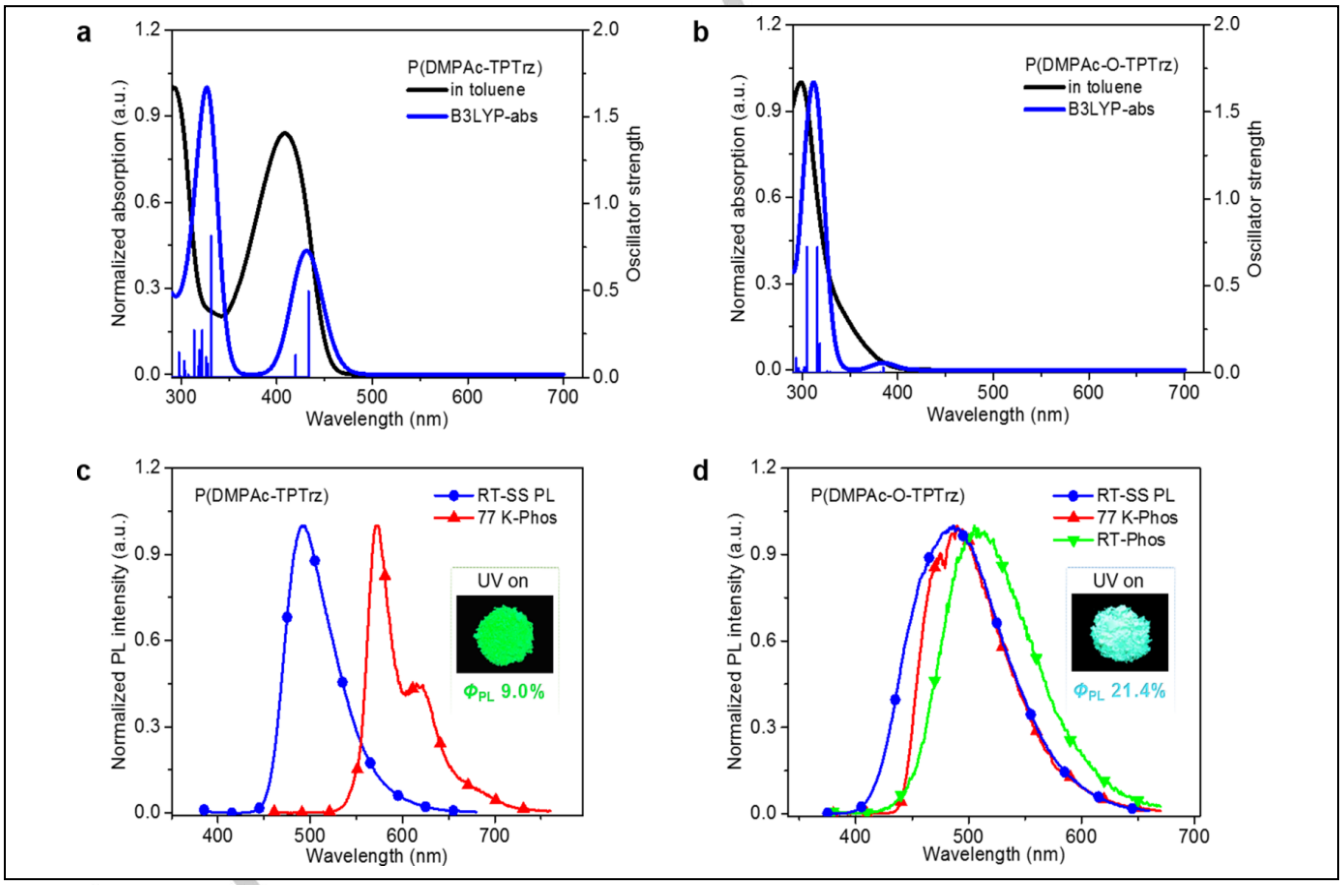

Figure 2. Absorption spectra measured in toluene (10^{-5} mol L^{-1}) (black curve) and the theoretical absorption spectra calculated at the B3LYP level (blue curve) of P(DMPAc-TPTrz) (a) and P(DMPAc-O-TPTrz) (b). Herein the discrete vertical lines illustrate the vertical excited energies (horizontal ordinate) and corresponding oscillator strengths (right ordinate). The steady-state PL spectra at room

temperature, and phosphorescence spectra at 77 K and room temperature for the neat films of P(DMPAc-TPTrz) (c) and P(DMPAc-O-TPTrz) (d). Inset: Corresponding photos with 365 nm UV lamp on.

2.3 Photophysical properties

Figure 2 shows the UV-Vis absorption in toluene, and steady-state photoluminescence (PL) and phosphorescent spectra in neat films for P(DMPAc-TPTrz) and P(DMPAc-O-TPTrz). As one can see, they both possess intense absorption bands below 370 nm, which can be reasonably ascribed to the local excited states (LE) from acridine and triazine fragments (Figure S4). Unlike P(DMPAc-TPTrz) with a distinct CT absorption peaked at 408 nm, only a long tail is observed in the range of 370-450 nm for P(DMPAc-O-TPTrz). According to the theoretical absorption, a hidden band of 384 nm does exist here, which turns out to be palpable with the increasing solution concentration (Figure S5). The related CT character is further confirmed by the positive solvatochromatic effect (Figure S6), and consistent with the separated HOMO and LUMO distributions (Figure S1). These observations suggest that, although a non-conjugated O atom is inserted between acridine and triazine, intramolecular CT can still be generated along the polymeric backbone in P(DMPAc-O-TPTrz).

The PL behavior of P(DMPAc-O-TPTrz) is then explored in neat film other than toluene solution because of its aggregation-induced emission (AIE) (Figure S7). Compared to the green P(DMPAc-TPTrz) with an emissive maximum of 491 nm and a PL quantum yield (PLQY) of 9.0%, P(DMPAc-O-TPTrz) displays a brighter sky-blue light with an emissive maximum of 486 nm and a PLQY of 21.4%. The hypochromatic shift is in well agreement with the optical and electrochemical bandgap (Table 1). Surprisingly, we note that the full-width at half-maximum (FWHM) is up from 61 nm of P(DMPAc-TPTrz) to 99 nm of P(DMPAc-O-TPTrz). Furthermore, P(DMPAc-TPTrz) has a phosphorescence merely at low temperature, whereas both low temperature phosphorescence and RTP could be monitored for P(DMPAc-O-TPTrz).

To explain the difference between P(DMPAc-TPTrz) and P(DMPAc-O-TPTrz), their time-resolved emission spectra (TRES) were measured at room temperature and plotted in Figure 3a-b. As for P(DMPAc-TPTrz), the corresponding spectral profile keeps almost unchanged with the varing delay time. Meanwhile, it looks like the same as the PL and deviates from the phosphorescence at 77 K, indicative of no RTP. On the contrary, the spectral profile of P(DMPAc-O-TPTrz) is obviously sensitive to the delay time. For example, at a short delay time of 0.1285 ns, P(DMPAc-O-TPTrz) exhibits a major peak around 450 nm accompanied by emission shoulders over 480 nm. As the delay time goes on, the former begins to disappear, and the latter becomes dominant in the whole TRES of P(DMPAc-O-TPTrz). Finally, it matches well with the phosphorescence spectra at room temperature, implying the existence of RTP in P(DMPAc-O-TPTrz).

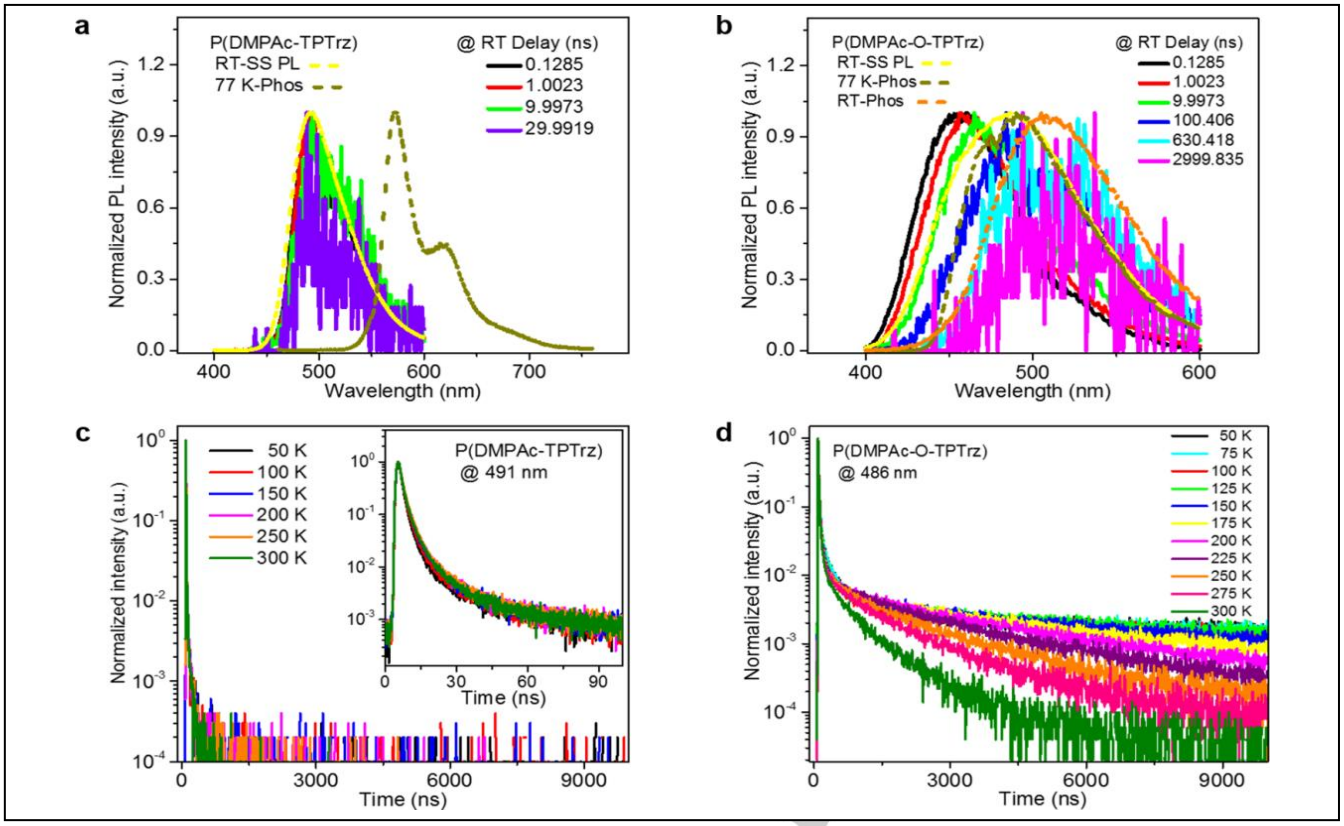

Figure 3. Time-resolved emission spectra at room temperature compared with steady-state PL, 77 K and room temperature phosphorescence for the neat films of P(DMPAc-TPTrz) (a) and P(DMPAc-O-TPTrz) (b), and temperature-dependent transient PL spectra for the neat films of P(DMPAc-TPTrz) (c) and P(DMPAc-O-TPTrz) (d).

To further verify the RTP nature, the temperature dependence on the transient PL spectra of P(DMPAc-O-TPTrz) were investigated with regard to P(DMPAc-TPTrz). As depicted in Figure 3c-d, P(DMPAc-TPTrz) displays merely prompt fluorescence without any thermally activated delayed fluorescence (TADF) or RTP signals. Combined with its corresponding TRES, P(DMPAc-TPTrz) is speculated as a typical fluor. By contrast, a significant delayed component can be recorded at the maximum emission of 486 nm for P(DMPAc-O-TPTrz), which correlates to RTP and behaves a negative temperature dependence. That is, when the temperature rises from 50 to 300 K, the delayed component is found to be monotonically decreased as a result of the elevated nonradiative decay.

Next, the detected wavelength is intentionally set to 425 nm, where the phosphorescence contribution is negligible (Figure S8). Under such a condition, noticeably, there is no delayed component in the temperature-insensitive decay curves of P(DMPAc-O-TPTrz). So the TADF influence is excluded reasonably[35], and we can deduce that the P(DMPAc-O-TPTrz) emission originates from both fluorescence and RTP. To decouple them from each other, a Bigaussian function is utilized to fit the neat film PL spectrum of P(DMPAc-O-TPTrz)[36]. And the fluorescence and RTP ratios are determined to be 48.8% and 51.2%, respectively, by comparing their individual integral area (Figure S11). This is responsible for the above-mentioned wider FWHM of P(DMPAc-O-TPTrz) relatively to P(DMPAc-TPTrz) showing only fluorescence. Also, the significant part of RTP obtained in P(DMPAc-O-TPTrz) can be attributed to the characteristic D-O-A geometry, which will be discussed below.

Meanwhile, the phosphorescence and steady-state PL spectra of the P(DMPAc-O-TPTrz) neat film are collected at different temperatures to further confirm whether RTP is the origin of the long-lived luminescence. As one can see in Figure S12a, the measured phosphorescence intensity turns out to get more and more intense without an obviuos significant spectral shift when temperature decreases from 300 to 77 K. This is in well agreement with the decoupled phosphorescence band via Bigaussian fitting of the steady-state PL spectra (Figure S13c), a good indicator of the RTP origin. And the observations in both cases could be attributed to the suppression of the molecular motions so that the portion of the lowest triplet state is expected to be increased due to the thermal equilibrium at low temperature[16].

Additionally, a similar RTP behavior is found when P(DMPAc-O-TPTrz) is dispersed into mCP (Figure S12b, S13b, S13d and S16-18). In this case, the unwanted triplet-triplet annihilation (TTA) could be eliminated, leading to a greatly reduced nonradiative decay rate constant of phosphorescence (k_{nr}^{P}) (Table S1: 1.1 × 10^{6}

s^{-1} Vs 0.41 × 10^6 s^{-1}). On going from neat to doped films, therefore, the PLQY and phosphorescence excited lifetime are enhanced from 21.4% and 825.4 ns to 49.5% and 1642.6 ns, respectively, associated with an improved RTP population from 51.2% to 65.0%.

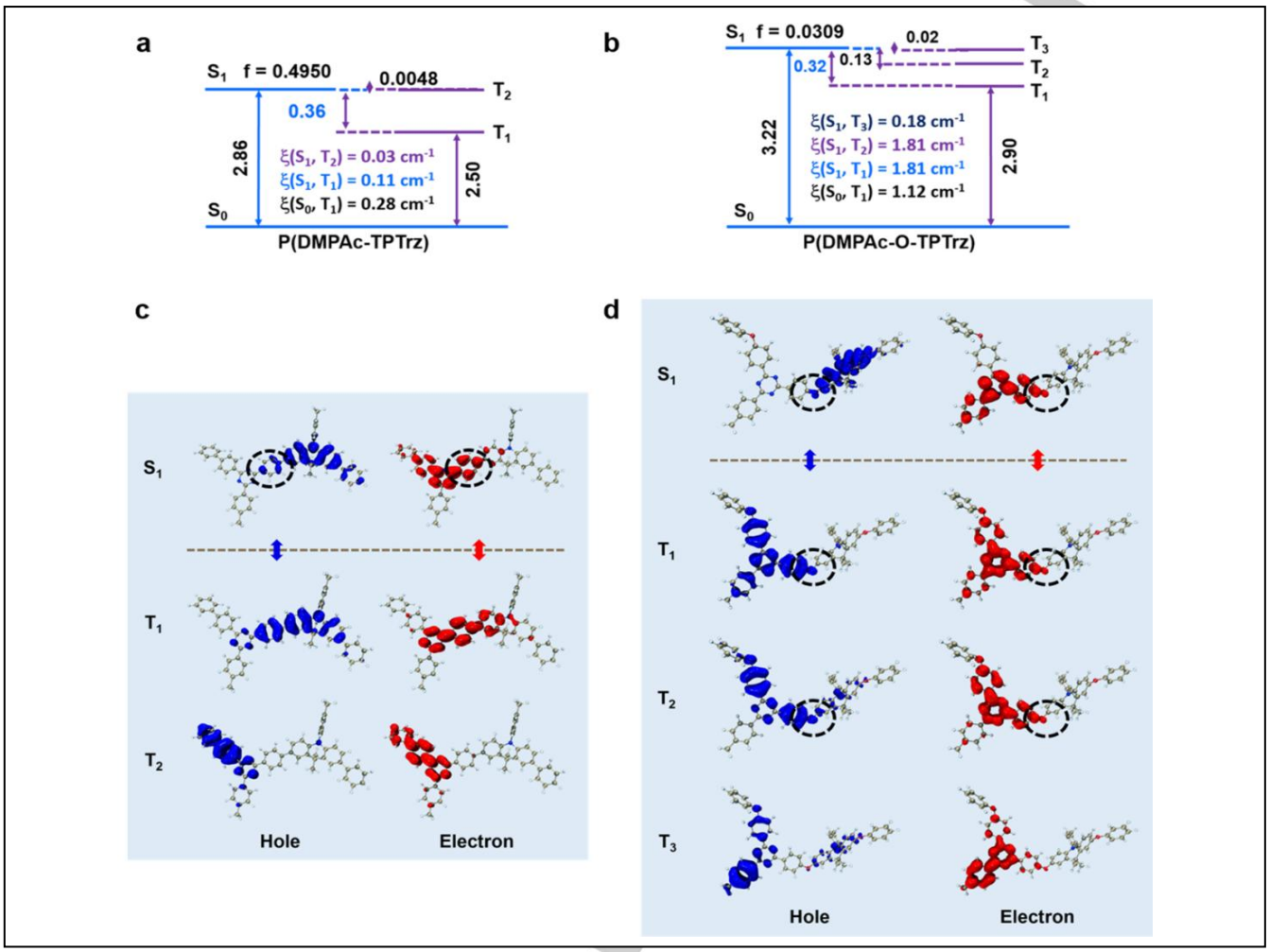

Figure 4. Energy level alignment together with the spin-orbit coupling matrix element and oscillator strength for P(DMPAc-TPTrz) (a) and P(DMPAc-O-TPTrz) (b), and hole and electron distributions of S_1 and T_n (below S_1) for P(DMPAc-TPTrz) (c) and P(DMPAc-O-TPTrz) (d).

2.4 Theoretical calculation

To identify the ISC and subsequent phosphorescence channels, theoretical calculations of P(DMPAc-TPTrz) and P(DMPAc-O-TPTrz) were carried out using Gaussian 09 package at a B3LYP/6-31G* level. As for P(DMPAc-O-TPTrz) (Figure 4a-b), there are three triplet states (T_1, T_2 and T_3) below the first singlet state (S_1), which have chances to be bestowed the excited state energy from S_1. The SOC matrix elements (SOCMEs) of the possible two ISC channels between S_1 and T_1, S_1 and T_2 are both predicted to be 1.81 cm^{-1}. And the SOCME between T_1 and S_0, corresponding to the phosphorescence channel, is on the same magnitude of 1.12 cm^{-1}. Compared with P(DMPAc-TPTrz), the correlated SOCMEs of P(DMPAc-O-TPTrz) are increased by about one order of magnitude, illustrating the strengthened SOC effect.

Furthermore, hole and electron were analysized to gain a clear insight into the role of the introduced O atom (Figure 4c-d). At first, the fluorescence process was investigated based on the hole and electron orbitals of S_1. It is found that, the overlap on the O atom in P(DMPAc-O-TPTrz) turns out to be smaller than that on the phenyl ring in P(DMPAc-TPTrz). As a result, a weakened fluorescence from S_1 to S_0 is anticipated for P(DMPAc-O-TPTrz), consistent with the much lower oscillator strength (f = 0.0309) relative to P(DMPAc-TPTrz) (f = 0.4950). In addition, the larger hole-electron separation leads to a decreased energy difference between S_1 and T_1 (ΔE_{ST} = 0.32 eV). Despite this, it is still big enough to prevent the thermally-aided up-conversion, and thus TADF is unlikely to happen as demonstrated before.

Subsequently, the ISC process was studied in terms of the orbital angular momentum change, which is related to charge migration from the hole orbital of S_1 to that of T_n and from the electron orbital of S_1 to that of T_n [37]. Since a similar electron distribution is observed for P(DMPAc-O-TPTrz), the ISC between

S_1 and T_1 or T_2 involves a certain degree of hole migration from acridine to triazine. Herein the introduced O is believed to have two influences. First, the dihedral angle between acridine and triazine is up from 29.5° of P(DMPAc-TPTrz) to 84.4° of P(DMPAc-O-TPTrz) (Figure S1). Second, attributable to the contributions of not only the lone pairs from O but also the delocalized π electrons from acridine or triazine, S_1, T_1 and T_2 bear the hybrid n-π* and π-π* characters. Both the elevated dihedral angle and n orbital contribution would induce a larger change of orbital angular momentum in P(DMPAc-O-TPTrz) than in P(DMPAc-TPTrz). According to the El-Sayed rule[38], the spin angular momentum can be compensated by the orbital angular momentum. Therefore, the spin-forbidden S_1-to-T_n (n = 1 and 2) flippings becomes favorable for P(DMPAc-O-TPTrz), in accordance with the increased SOCMEs. Following the same rule, the phosphorescence process from T_1 to S_0 is also able to be favored, given that the corresponding hole and electron orbitals of T_1 are contributed by the n orbital of O to some degree.

Together with the photophysical results, the light-emitting mechanism of P(DMPAc-O-TPTrz) is tentatively proposed as follows (Figure S19). Under photo excitation, the singlet excitons are produced at beginning. On one hand, the O insertion between D and A causes a smaller hole-electron overlap in S_1. Hence its radiative decay is lowered, resulting in a weak CT fluorescence. This is in contrast to the strong fluorescence for P(DMPAc-TPTrz). On the other hand, as a competitive process, the ISC between S_1 and T_n (n = 1 and 2) is promoted by the strengthened SOC effect from O, followed by an effective T_1-to-S_0 phosphorescence channel. Consequently, P(DMPAc-O-TPTrz) can emit a considerable RTP rather than P(DMPAc-TPTrz). It should be noted that all these processes occur in the solid state, where the rigid environment is required for the restraint of molecular motion and thus generation of RTP. Moreover, the difference between P(DMPAc-TPTrz) and P(DMPAc-O-TPTrz) clearly highlights that the D-O-A geometry is superior to the D-A one for the development of electro-active RTP polymers.

2.5 PLEDs application

In view of the electro-active feature, considerable RTP, moderate PLQY and microsecond lifetime, P(DMPAc-O-TPTrz) does have a great potential for PLEDs. To evaluate this point, PLEDs were fabricated with a configuration of ITO/PEDOT:PSS (40 nm)/mCP:P(DMPAc-O-TPTrz) (30 nm)/TSPO1 (8 nm)/TmPyPB (42 nm)/LiF (1 nm)/Al (100 nm) (Figure 5a). Herein PEDOT:PSS (Clevios P AI4083), TSPO1 and TmPyPB are used as the hole injection layer, exciton blocking layer and electron transporting layer, respectively. And the emitting layer is composed of mCP doped with 15 wt.% P(DMPAc-O-TPTrz) to avoid TTA. For reference, a control device is also fabricated with P(DMPAc-TPTrz) as the dopant instead of P(DMPAc-O-TPTrz).

Similar to their PL counterparts, the electroluminescence (EL) spectrum of P(DMPAc-O-TPTrz) is found to be much broader than that of P(DMPAc-TPTrz) (Figure 5b). This means that RTP and fluorescence both contribute to the EL process of P(DMPAc-O-TPTrz) (Figure S21). Under photo excitation, triplet excitons must be produced only through ISC. And the ISC probility is reasonably set to be the same as that of the RTP population (65.0%). Under electric excitation, however, 75% triplet excitons are directly generated from the injected holes and electrons, and 25% singlet excitons can spin-flip to form 16.3% triplet excitons assuming a same ISC probability as the PL process. In all, a total of 91.3% triplet excitons is involved during the EL process. The improved RTP population is further proved by the enhancement of the FWHM from 91 nm of the PL spectrum to 118 nm of the EL spectrum (Figure S22).

Different from the previously-reported insulating RTP polymers, P(DMPAc-O-TPTrz) possesses a good electroactivity in redox, which is capable of charge transporting. So the P(DMPAc-O-TPTrz) based device presents a moderate current density and luminance (Figure 5c-d). Meanwhile, the device reaches a peak EQE of 7.9% (20.2 cd/A, 12.7 lm/W), more than double that of P(DMPAc-TPTrz) (3.3%, 8.6 cd/A, 5.4 lm/W). Owing to the microsecond lifetime, a less efficiency roll-off is obtained at high luminance. For instance, the EQE still remains to 7.3% even at 1000 cd/m^2. When PEDOT:PSS (Clevios P CH8000) with a lower conductivity is adopted as the hole injection layer, the EQE can be further optimized to 9.7% (24.0 cd/A, 18.9 lm/W) along with CIE coordinates of (0.27, 0.41) (Figure 6). Noticeably, the performance is well beyond the 5% theoretical limit for fluorescent PLEDs[39], because both singlet and triplet excitons can be simultaneously harvested in P(DMPAc-O-TPTrz). To the best of our knowledge, this is the first example of pure organic RTP polymers towards highly efficient PLEDs.

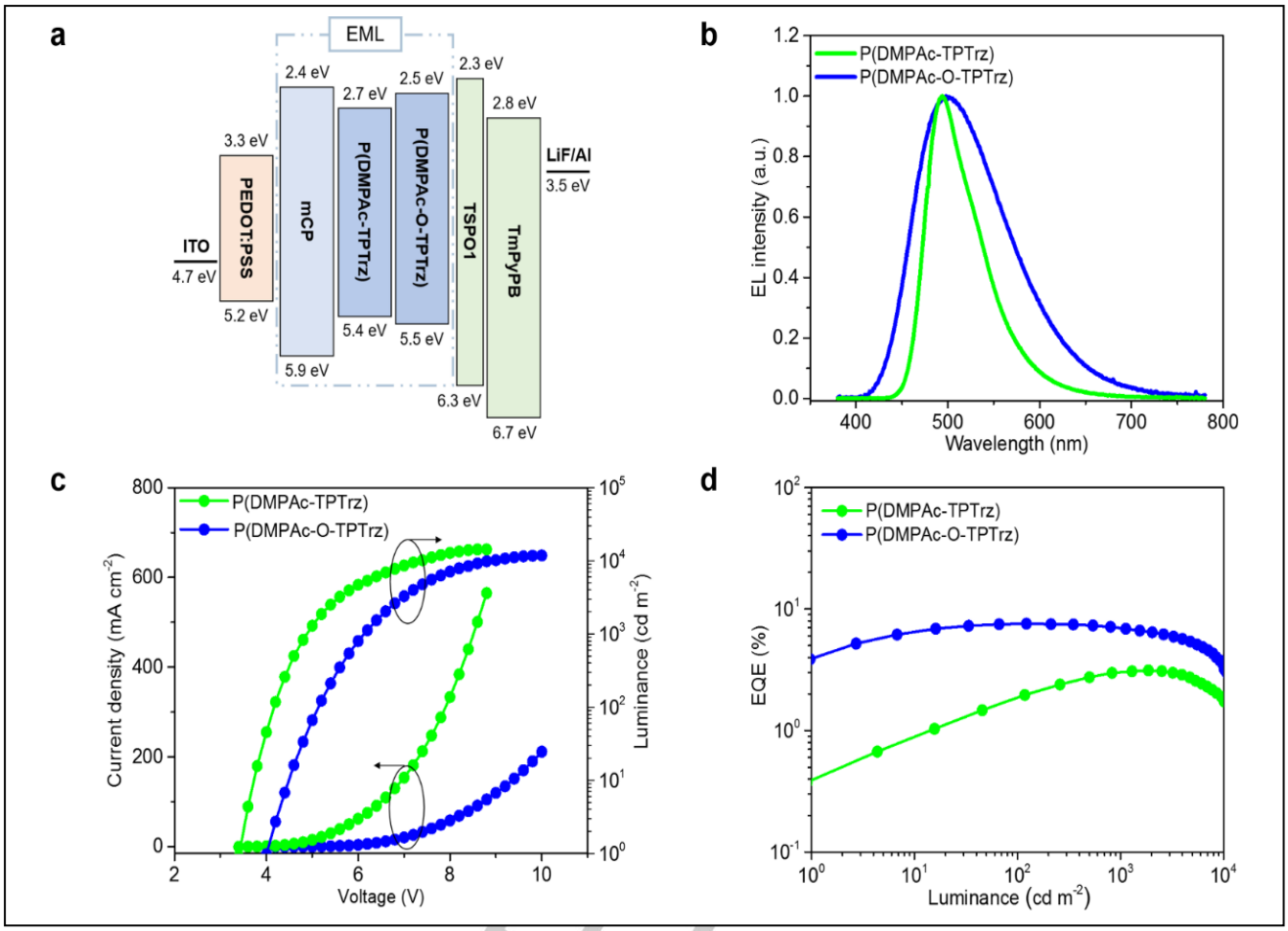

Figure 5. Device performance for P(DMPAc-TPTrz) and P(DMPAc-O-TPTrz) with PEDOT:PSS (Clevios P AI4083) as the hole injection layer: (a) Device structure and related energy level diagram; (b) EL spectra; (c) Current density-voltage-luminance characteristics; (d) EQE as a function of luminance.

Table 2. Device performance of P(DMPAc-TPTrz) and P(DMPAc-O-TPTrz) based PLEDs.

Device	V_{on} [c] [V]	CE [d] [cd/A]	PE [d] [lm/W]	EQE [d] [%]	λ_{EL} [e] [nm]	CIE [f] [x, y]
P(DMPAc-TPTrz) [a]	3.6	8.6	5.4	3.3	494 (65)	(0.20, 0.49)
P(DMPAc-O-TPTrz) [a]	4.2	20.2	12.7	7.9	498 (118)	(0.26, 0.42)
P(DMPAc-O-TPTrz) [b]	3.7	24.0	18.9	9.7	495 (119)	(0.27, 0.41)

[a]With PEDOT:PSS (Clevios P AI4083) as the hole injection layer. [b]With PEDOT:PSS (Clevios P CH8000) as the hole injection layer. [c]Turn-on voltage at 1 cd/m^2. [d]Maximum data. [e]EL maxima at 1000 cd/m^2 and the corresponding FWHM listed in the parentheses. [f]CIE 1931 coordinates. CE, current efficiency. PE, power efficiency.

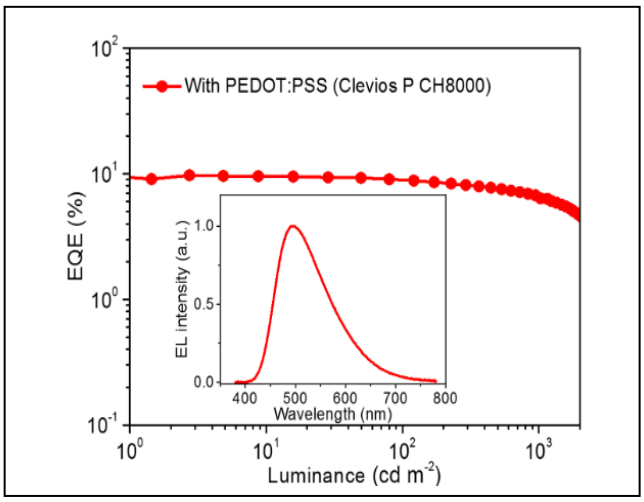

Figure 6. EQE as a function of luminance for P(DMPAc-O-TPTrz) with PEDOT:PSS (Clevios P CH8000) as the hole injection layer. Inset: EL spectrum.

3. Conclusion

In summary, an electro-active RTP polymer, namely P(DMPAc-O-TPTrz), has been designed and synthesized on the basis of a characteristic D-O-A geometry. Compared with the D-A based P(DMPAc-TPTrz), the inserted O in P(DMPAc-O-TPTrz) suppresses CT fluorescence as a result of a decreased hole-electron orbital overlap. On the other hand, the S_1-to-T_n ISC and subsequent T_1-to-S_0 phosphorescence channels can be promoted by a strengthened SOC effect due to the n-orbital contribution and large dihedral angle between D and A. Consequently, a significant RTP in solid states is achieved for P(DMPAc-O-TPTrz), whose electrophosphorescence devices show a promising EQE of 9.7%. This work, we believe, will open a new door to develop next generation pure organic RTP PLEDs with high-performance and low-cost.

4. Experimental Section

The supplementary materials for this paper include experimental section; synthetic and characterization data (^{1}H and ^{13}C NMR spectra) for each intermediate and final polymer; theoretical calculation; and thermal, electrochemical, photophysical and device data.

ORCID

Junqiao Ding: 0000-0001-7719-6599

Notes

The authors declare no competing financial interest.

Acknowledgements

The authors acknowledge the National Natural Science Foundation of China (Nos. 51873205 and 51703223), and the National Key Research and Development Program (2016YFB0401301) for the financial support.

Keywords: Pure organic room-temperature phosphorescence; polymer light-emitting diodes; donor-oxygen-acceptor; electro-active; electrophosphorescence

References:

1. S. Mukherjee, P. Thilagar, *Chem. Commun.* **2015**, *51*, 10988.
2. Kenry, C. Chen, B. Liu, *Nat. Commun.* **2019**, *10*, 2111.
3. S. Xu, R. Chen, C. Zheng, W. Huang, *Adv. Mater.* **2016**, *28*, 9920.
4. R. Kabe, C. Adachi, *Nature* **2017**, *550*, 384.
5. S. Hirata, *Adv. Opt. Mater.* **2017**, *5*, 1700116.
6. O. Bolton, K. Lee, H.-J. Kim, K. Y. Lin, J. Kim, *Nat. Chem.* **2011**, *3*, 205.
7. O. Bolton, D. Lee, J. Jung, J. Kim, *Chem. Mater.* **2014**, *26*, 6644.
8. S. Cai, H. Shi, D. Tian, H. Ma, Z. Cheng, Q. Wu, M. Gu, L. Huang, Z. An, Q. Peng, W. Huang, *Adv. Funct. Mater.* **2018**, *28*, 1705045.
9. L. Gu, H. Shi, C. Miao, Q. Wu, Z. Cheng, S. Cai, M. Gu, C. Ma, W. Yao, Y. Gao, Z. An, W. Huang, *J. Mater. Chem. C* **2018**, *6*, 226.
10. W. Z. Yuan, X. Y. Shen, H. Zhao, J. W. Y. Lam, L. Tang, P. Lu, C. Wang, Y. Liu, Z. Wang, Q. Zheng, J. Z. Sun, Y. Ma, B. Z. Tang, *J. Phys. Chem. C* **2010**, *114*, 6090.
11. L. Xu, K. Zhou, H. Ma, A. Lv, D. Pei, G. Li, Y. Zhang, Z. An, A. Li, G. He, *ACS Appl. Mater. Interfaces* **2020**, *12*, 18385.
12. Z. An, C. Zheng, Y. Tao, R. Chen, H. Shi, T. Chen, Z. Wang, H. Li, R. Deng, X. Liu, W. Huang, *Nat. Mater.* **2015**, *14*, 685.
13. S. Cai, H. Shi, J. Li, L. Gu, Y. Ni, Z. Cheng, S. Wang, W.-W. Xiong, L. Li, Z. An, W. Huang, *Adv. Mater.* **2017**, *29*, 1701244.
14. E. Lucenti, A. Forni, C. Botta, L. Carlucci, C. Giannini, D. Marinotto, A. Previtali, S. Righetto, E. Cariati, *J. Phys. Chem. Lett.* **2017**, *8*, 1894.
15. W. Zhao, Z. He, J. W. Y. Lam, Q. Peng, H. Ma, Z. Shuai, G. Bai, J. Hao, B. Z. Tang, *Chem* **2016**, *1*, 592.
16. Z. He, W. Zhao, J. W. Y. Lam, Q. Peng, H. Ma, G. Liang, Z. Shuai, B. Z. Tang, *Nat. Commun.* **2017**, *8*, 416.
17. T. Zhang, X. Ma, H. Wu, L. Zhu, Y. Zhao, H. Tian, *Angew. Chem. Int. Ed.* **2020**, *59*, 11206.
18. J. Wang, J. Liang, Y. Xu, B. Liang, J. Wei, C. Li, X. Mu, K. Ye, Y. Wang, *J. Phys. Chem. Lett.* **2019**, *10*, 5983.
19. Y. Su, S. Z. F. Phua, Y. Li, X. Zhou, D. Jana, G. Liu, W. Q. Lim, W. K. Ong, C. Yang, Y. Zhao, *Sci. Adv.* **2018**, *4*, eaas9732.
20. M.-M. Fang, J. Yang, Z. Li, *Chin. J. Polym. Sci.* **2019**, *37*, 383.
21. N. Gan, H. Shi, Z. An, W. Huang, *Adv. Funct. Mater.* **2018**,

28, 1802657.
22. H. Wang, H. Shi, W. Ye, X. Yao, Q. Wang, C. Dong, W. Jia, H. Ma, S. Cai, K. Huang, L. Fu, Y. Zhang, J. Zhi, L. Gu, Y. Zhao, Z. An, W. Huang, *Angew. Chem. Int. Ed.* **2019**, *58*, 18776.
23. D. Lee, O. Bolton, B. C. Kim, J. H. Youk, S. Takayama, J. Kim, *J. Am. Chem. Soc.* **2013**, *135*, 6325.
24. M. S. Kwon, Y. Yu, C. Coburn, A. W. Phillips, K. Chung, A. Shanker, J. Jung, G. Kim, K. Pipe, S. R. Forrest, J. H. Youk, J. Gierschner, J. Kim, *Nat. Commun.* **2015**, *6*, 8947.
25. M. S. Kwon, D. Lee, S. Seo, J. Jung, J. Kim, *Angew. Chem. Int. Ed.* **2014**, *53*, 11177.
26. G. Zhang, J. Chen, S. J. Payne, S. E. Kooi, J. N. Demas, C. L. Fraser, *J. Am. Chem. Soc.* **2007**, *129*, 8942.
27. C. A. DeRosa, C. Kerr, Z. Fan, M. Kolpaczynska, A. S. Mathew, R. E. Evans, G. Zhang, C. L. Fraser, *ACS Appl. Mater. Interfaces* **2015**, *7*, 23633.
28. H. Chen, X. Yao, X. Ma, H. Tian, *Adv. Optical Mater.* **2016**, *4*, 1397.
29. X. Ma, C. Xu, J. Wang, H. Tian, *Angew. Chem. Int. Ed.* **2018**, *57*, 10854.
30. Y. He, N. Cheng, X. Xu, J. Fu, J.-A. Wang, *Org. Electron.* **2019**, *64*, 247.
31. A. C. Grimsdale, K. L. Chan, R. E. Martin, P. G. Jokisz, A. B. Holmes, *Chem. Rev.* **2009**, *109*, 897.
32. X. Liu, J. Rao, X. Li, S. Wang, J. Ding, L. Wang, *iScience* **2019**, *15*, 147.
33. J. Rao, X. Liu, X. Li, L. Yang, L. Zhao, S. Wang, J. Ding, L. Wang, *Angew. Chem. Int. Ed.* **2020**, *59*, 1320.
34. Y. Wang, S. Wang, N. Zhao, B. Gao, S. Shao, J. Ding, L. Wang, X. Jing, F. Wang, *Polym. Chem.* **2015**, *6*, 1180.
35. H. Uoyama, K. Goushi, K. Shizu, H. Nomura, C. Adachi, *Nature* **2012**, *492*, 234.
36. Y. Tang, G. Xie, X. Yin, Y. Gao, J. Ding, C. Yang, *J. Phys. Chem. Lett.* **2020**, *11*, 5255.
37. D. R. Lee, K. H. Lee, W. Shao, C. L. Kim, J. Kim, J. Y. Lee, *Chem. Mater.* **2020**, *32*, 2583.
38. M. A. El-Sayed, *J. Chem. Phys.* **1963**, *38*, 2834.
39. Y. Cao, I. D. Parker, G. Yu, C. Zhang, A. J. Heeger, *Nature* **1999**, *397*, 414.

10.1002/anie.202011957

WILEY-VCH

Entry for the Table of Contents (Please choose one layout)

Layout 2:

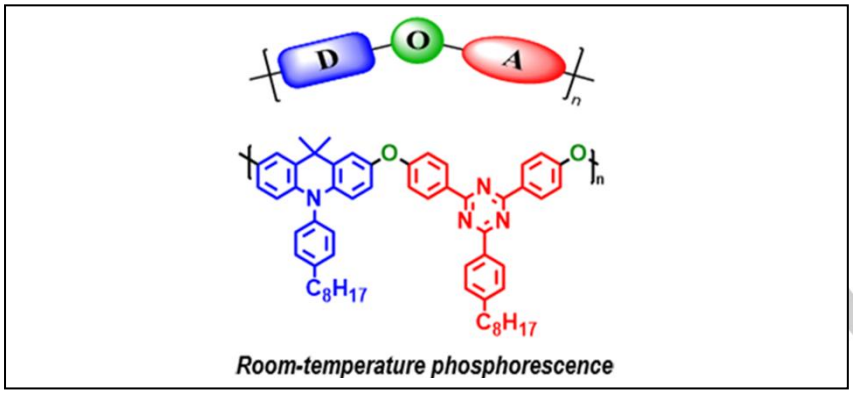

X. Liu, L. Yang, X. Li, L. Zhao, S. Wang, Z.-H. Lu*, J. Ding* and L. Wang*

Page No. – Page No.

Electro-active pure organic room-temperature phosphorescence polymer based on a donor-oxygen-acceptor geometry

A donor-oxygen-acceptor geometry has been demonstrated for the design of electro-active pure organic room-temperature phosphorescence polymers, whose PLEDs achieve a promising EQE of 9.7%.